In situ annealing of nanoporous silicon thin films with transmission electron microscopy

Li, Qin-Yi
Department of Aeronautics and Astronautics, Kyushu University

Fabian Javier Medina
Department of Aerospace and Mechanical Engineering, University of Arizona

Kokura, Kosuke
Department of Aeronautics and Astronautics, Kyushu University

Jin, Zheyu
Department of Aeronautics and Astronautics, Kyushu University

他

出版情報：Applied physics letters. 123 (24), pp.241601-, 2023-12-11. AIP Publishing
バージョン：

In-Situ Annealing of Nanoporous Silicon Thin Films with Transmission Electron Microscopy

Qin-Yi Li[1,3,*], Fabian Javier Medina[2], Kosuke Kokura[1], Zheyu Jin[1], Koji Takahashi[1,3], Qing Hao[2,*]

[1]*Department of Aeronautics and Astronautics, Kyushu University, 744 Motooka, Fukuoka 819-0395, Japan*

[2]*Department of Aerospace and Mechanical Engineering, University of Arizona, Tucson, AZ 85721, USA*

[3]*International Institute for Carbon-Neutral Energy Research (WPI-I2CNER), Kyushu University, 744 Motooka, Fukuoka 819-0395, Japan*

Corresponding authors: Qing Hao: qinghao@email.arizona.edu;

Qin-Yi Li: qinyi.li@aero.kyushu-u.ac.jp

Abstract

Nanoporous films have potential applications in thermoelectric cooling on a chip, sensors, solar cells, and desalination. For phonon transport, amorphization and other pore-edge defects introduced by the nanofabrication processes can eliminate wave effects by diffusively scattering short-wavelength phonons and thus destroying the phonon phase coherence. As a result, phononic effects can only be observed at 10 K or below, when long-wavelength phonons become dominant for thermal transport. In this work, a 70-nm-thick silicon thin film with approximately 100-nm-diameter nanopores was annealed under a high vacuum and the change of pore-edge defects was observed with *in-situ* transmission electron microscopy. It was found that the pore-edge defects can be minimized to a sub-1-nm layer by annealing between 773 K and 873 K for 30 minutes,

without changing the pore sizes. The largely reduced pore-edge defects are critical to the desired phonon wave effects within a periodic nanoporous structure.

Main Text

Nanoporous thin films have wide applications in heat manipulation,[1-3] thermoelectrics,[4, 5] sensors,[6] solar cells,[7] and water desalination.[8] For applications such as thermoelectrics, "phononic crystals" based on phonon wave effects have been intensively studied in recent years, as the thermal analogy to photonic crystals.[1-4] Examples include superlattice thin films and periodic nanoporous structures. In these structures, the backward reflected lattice vibration waves by periodic interfaces or boundaries would interfere with the forward waves, which can largely change the phonon behavior for heat manipulation. Such phononic effects have been intensively studied for superlattice thin films with atomically smooth interfaces between alternating layers. In experiments, it has been found that coherent phonon transport becomes dominant for <5 nm periods at 300 K.[9, 10] For periodic nanoporous thin films, comparable smooth pore edges cannot be obtained by the employed pore-drilling techniques such as dry etching or a focused ion beam (FIB). In transmission electron microscopy (TEM) studies, a 2-nm-thick amorphization and oxidation layer can often be found at the pore edges.[11] The pore-edge roughness is comparable to the phonon wavelengths of 1–10 nm for Si at 300 K.[12, 13] The resulting diffusive pore-edge phonon scattering can destroy the phonon phase and thus phononic effects at room temperature. In practice, the pore-edge defects would effectively expand the pore diameters.[13, 14] In comparison experiments between ordered and disordered nanoporous patterns, the wave effects become critical only at a temperature T of ~10 K or below.[1, 15] At such a low temperature, the dominant phonon wavelength, $\lambda \sim 1/T$,[16] becomes much longer than the pore-edge roughness and specular pore-edge phonon

takes place to ensure coherent phonon transport. Along this line, reducing pore-edge defects is of significance to the manipulation of phonon transport though such issues are less important for photonic crystals manipulating photons with much longer wavelengths.

Without drilling or etching nanopores, pore-edge defects can be minimized by directly growing nanoporous $In_{0.1}Ga_{0.9}N$ films with SiO_2 nanopillars as masks for metal-organic chemical vapor deposition.[17] As another common practice, annealing may also be considered as an effective way to remove pore-edge defects. The reconstruction of carbon atoms at the edge of a hole[18] or a nanoribbon[19] has been observed under electron beam irradiation or Joule heating within graphene by TEM, which has offered significant insights into the phonon transport studies on graphene nanoribbons or nanoporous graphene.[4, 5, 20-23] However, particular attention should be paid to the possible shape variation of the nanoporous films at an elevated temperature.[18, 24-26] Besides phonon transport, annealing can also impact the photoluminescence properties of nanoporous Si. For instance, a significant reduction of photoluminescence intensity was observed for annealing temperatures above 473 K.[27] Another study showed photoluminescence quenching of nanoporous Si after annealing at 623 K in N_2 gas, which was associated with the structural changes and dangling bond formations at pore edges.[28] Despite these early studies, the exact pore-edge atomic structure variation has not been obtained for nanoporous Si, which hinders a better understanding of the annealing effect.

In this work, *in-situ* TEM studies were performed to track the pore-edge atomic structure variation within a nanoporous Si thin film during the annealing process under a high vacuum of ~10^{-5} Pa, which revealed the reduction of the amorphous layer and other pore-edge defects with this approach. It was found that annealing between 773 K and 873 K for 30 minutes can effectively minimize the pore-edge defects but still maintain the nanopore shapes. Our results provide

important guidance for how to fabricate high-quality nanoporous thin films for thermal and optical applications.

As shown in Figure 1(a), we fabricated nanoporous silicon thin films from the 70-nm-thick single-crystal silicon layer of commercial silicon-on-insulator (SOI) wafers using the polystyrene nanospheres (PSNS) based nanosphere lithography method.[14] The obtained pore diameters ranged from ~50 nm to ~130 nm, with the pitch averaging around 160 nm. The nanoporous 70-nanometer-thick silicon thin films were released from the substrate by etching away the buried oxide layer using diluted hydrofluoric (HF) acid, with the protection by a coated polymethyl methacrylate (PMMA) layer. They were subsequently transferred onto a commercial MEMS heating chip with through-holes (DENS solutions Wildfire Nano-Chip) and then subjected to PMMA removal, leaving a suspended nanoporous thin film, as displayed in Figure 1(e), for observation using TEM (JEM-2100Plus, JEOL) with a 200 kV acceleration voltage. More details of the sample preparation procedures are provided in Supplementary Note 1. Figures 1(b) and (c) display the EDS (energy dispersive X-ray spectroscopy) mapping of the silicon element and the EDS spectrum of the nanoporous silicon thin film, respectively, the latter of which reveals a small amount of oxidation.

As depicted in Figure 1(d), our *in-situ* annealing process started at 295 K, gradually raising the sample's temperature to 623 K over a duration of 1,968 seconds. Subsequently, we conducted sequential annealing steps at 673 K, 723 K, 773 K, 823 K, and 873 K, each lasting for 30 minutes, with a heating rate of 5 K/min between each temperature transition. The maximum annealing temperature (873 K) represented approximately half of the bulk silicon's melting point (1683 K)[29]. TEM images were captured following annealing at each specified temperature. Figure 1(g) illustrates the evolution of TEM images for a representative silicon nanopore as the temperature increased from 295 K to 873 K. These images clearly depict the contraction of the amorphous edge

and its partial transformation into a crystalline structure after annealing. Figure 1(f) presents the fast Fourier transform (FFT) pattern derived from the TEM image of the silicon thin film. This pattern enabled us to ascertain the crystal orientation as [1 0 0] and determine the lattice constant as 0.191 nm. Additionally, Supplementary Figure S6 offers a plot of the measured lattice constant versus the annealing temperature, revealing negligible variation in lattice spacing throughout the annealing process.

We monitored the evolution of atomic structures along the edges of four representative nanopores, as illustrated in Figure 2. Figures 2(a) to (d) display TEM images and the dimensions of the amorphous edge at specific positions, captured at 295 K for Pore-1 to Pore-3 and at 623 K for Pore-4 (TEM images of Pore-4 at 295 K were not obtained). In contrast, Figures 2(e) to (h) show TEM images and the amorphous edge dimensions at the same positions at 873 K for Pore-1 to Pore-4, respectively. These TEM images demonstrate that the widths of the defective pore edges were reduced from 2−3 nm to approximately 1 nm after the annealing process.

Given the non-uniform distribution of pore-edge defects around each pore, we measured the sizes of the defective pore edges at ten or more positions along the circumference. The average sizes of the amorphous pore edges for Pore-1 to Pore-4 are presented in Figures 2(i) to (l), respectively, along with error bars representing the standard deviations. All TEM images and positions used for the pore-edge size measurements can be found in Supplementary Note 2. The dimensions of the amorphous pore edges reached their minimum value of approximately 1 nm after annealing at 773 K for 30 minutes, with slight variations observed between 773 K and 873 K. This suggests that the minimal sub-1-nm-wide amorphous edge could be the limit in the annealing process, potentially due to the small amount of inevitable oxidation as well as some hydrogen termination initially. [30] Considering that the pore neck is approximately 20 nm in width,

the reduction in the dimensions of the amorphous edges by approximately 2 nm constitutes a significant change, equivalent to about one-tenth of the pore neck's width, which can result in noteworthy modification in the thermal and optical properties of the nanoporous thin film.

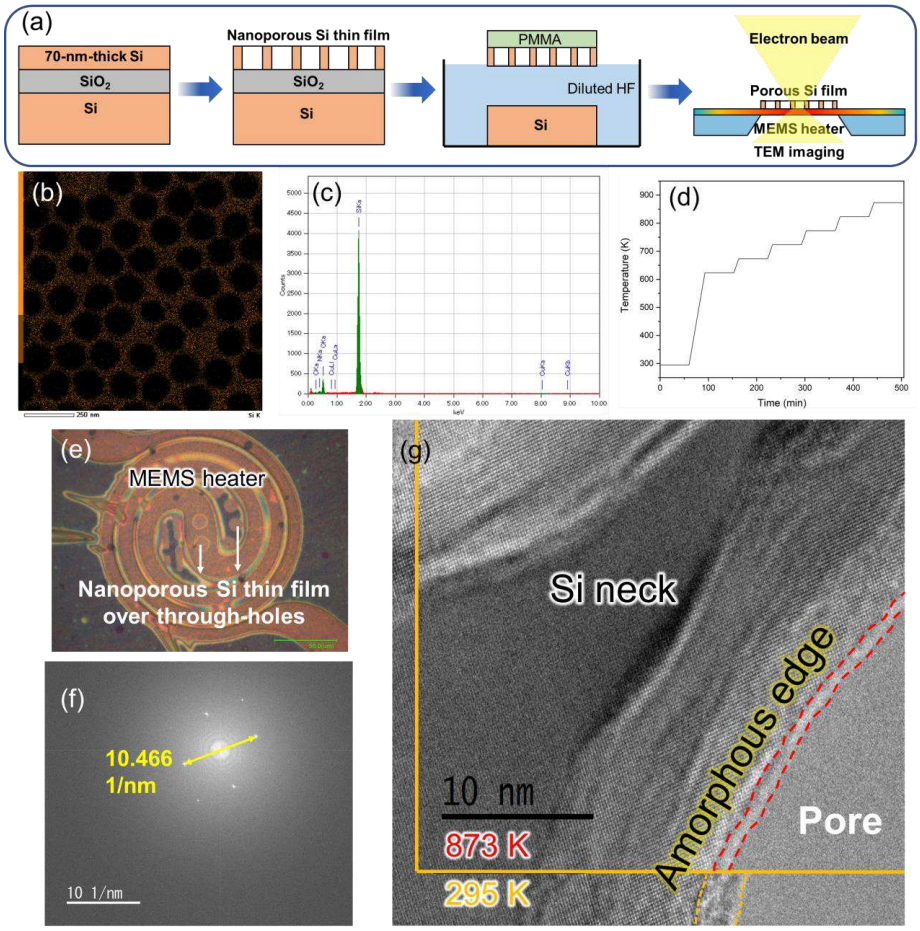

Figure 1 Experimental procedure and sample characterization. (a) Sample fabrication processes. (b) Silicon elemental mapping with EDS of the nanoporous thin film. (c) EDS spectrum of the nanoporous thin film. (d) Temperature history during the *in-situ* TEM observation. (e) Optical image

of the nanoporous Si thin film on the MEMS heater. (f) Fast Fourier transform (FFT) pattern derived from the TEM image of the nanoporous silicon thin film. (g) Structural change of a typical pore edge at 295 K and 873 K.

During the annealing process, the silicon atoms at the amorphous edge gain thermal energy and evaporate or transform to crystalline structures.[18, 19] The rate of the edge reconstruction depends on the energy barrier for migration of a silicon atom, denoted by E_b, with an exponential relationship of ~exp($-E_b/k_BT$), where k_B is the Boltzmann constant, and T is the annealing temperature.[18, 31] Thus, we can estimate the width of the amorphous pore edge, d, by an expression of $d = d_0[1\text{-exp}(-E_b/k_BT)]$, where d_0 is the initial width of the amorphous edge. We use this expression to fit the measured amorphous widths for Pore-1 to Pore-3 in Figs. 2(i) to (k), where the red curves present the fitting results. For Pore-4, we could not fit for the migration energy barrier due to the lack of room-temperature data. If we express the migration energy barrier in terms of the Boltzmann constant as $E_b = k_BT_b$, the exponential fitting gives T_b = 275 K for Pore-1, 182 K for Pore-2, and 591 K for Pore-3, while d_0 = 4.76 nm for Pore-1, 7.36 nm for Pore-2, and 3.36 nm for Pore-3.

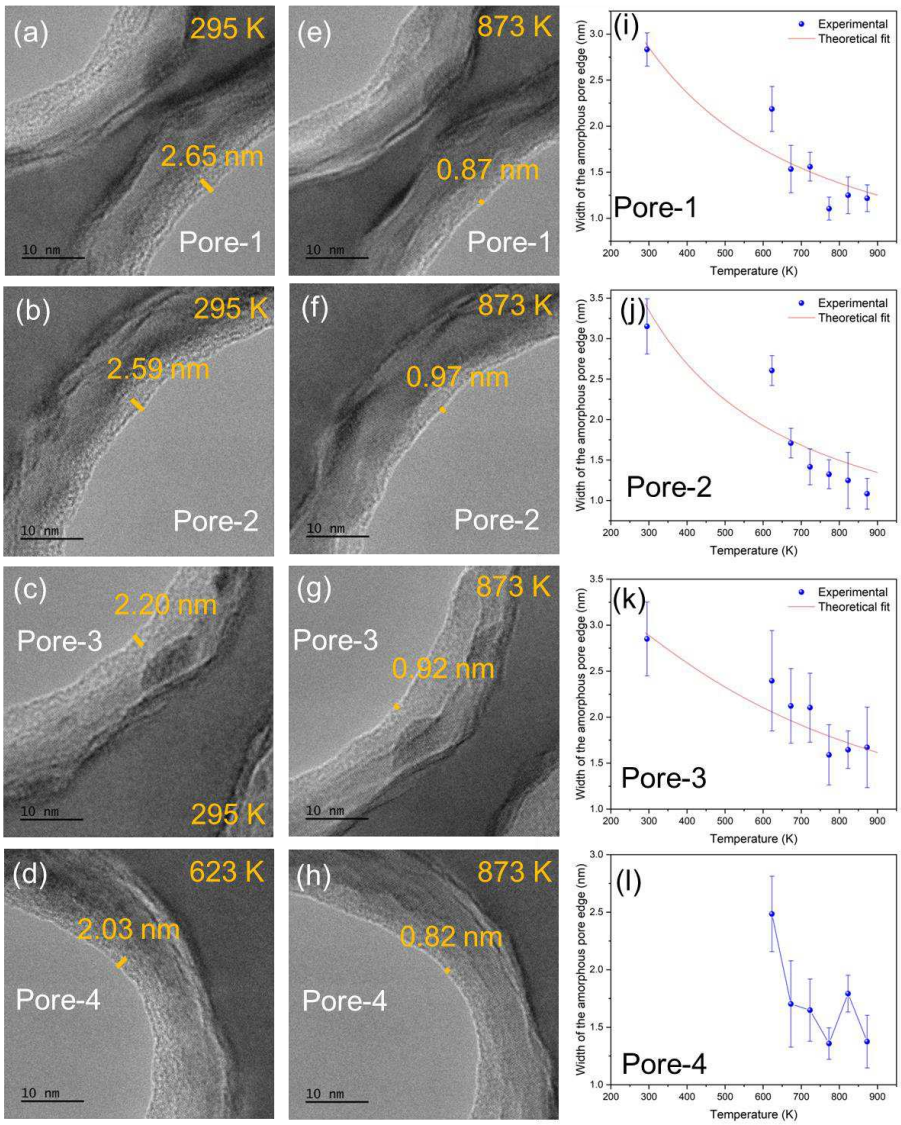

Figure 2 The defected pore edges changing with the annealing temperature. (a)-(c): TEM images of the edges of Pore-1, Pore-2, and Pore-3 at 295 K; (d): TEM image of the edge of Pore-4 at 623 K; (TEM images of Pore-4 at room temperature were not captured.) (e)-(h): TEM images of the edges

of Pore-1 ~ Pore-4 at 873 K; (i)-(l): the characteristic sizes of the defected pore edges changing with the annealing temperatures for Pore-1 to Pore-4 along with the theoretical fitting curves with the defect migration energy barriers for Pore-1 to Pore-3.

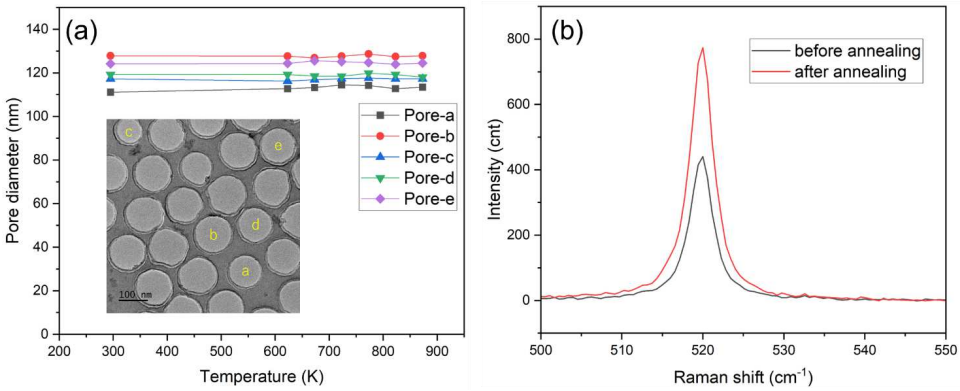

Figure 3 (a) Diameters of representative nanopores changing with the annealing temperature, inset of (a) illustrates the studied Pore-a to Pore-e; (b) Raman spectra of the nanoporous silicon thin film before and after annealing.

We examined whether the pore shape underwent any change during the annealing process and monitored the evolution of pore diameter for five representative pores, labeled as Pore-a to Pore-e in the inset of Figure 3(a), at each annealing temperature. Since the pore's shape closely resembles that of a truncated cone, we determined the pore diameter as the average value of the inner and outer diameters, as depicted in Supplementary Note 3. As demonstrated in Figure 3(a), the diameters of these five nanopores, ranging from approximately 110 nm to 130 nm, exhibited no significant variations throughout the entire annealing process, spanning from room temperature to 873 K. Consequently, we achieved a reduction in the dimensions of the amorphous pore edges without altering the overall pore shape.

We also examined the Raman spectra of the nanoporous silicon thin film before and after the *in-situ* annealing process using a 488 nm laser, as shown in Figure 3(b). The Raman shifts of the nanoporous thin film exhibited minimal change, shifting from 519.85 cm^{-1} before annealing to 519.81 cm^{-1} after annealing. However, the full width at half maximum (FWHM) reduced from 3.43 cm^{-1} before annealing to 3.35 cm^{-1} after annealing, and the intensity nearly doubled, increasing from 437 counts to 774 counts after annealing. The changes in the Raman peak intensity and the FWHM suggest the crystallization of the amorphous pore edges and a decrease in defects within the pore necks after the *in-situ* annealing in TEM.

In summary, we conducted *in-situ* annealing of a 70-nm-thick nanoporous silicon thin film within the high-vacuum environment of TEM, thus preventing contamination and oxidation throughout the entire annealing procedure. The studied nanopores had diameters of approximately 120 nm, with pore necks measuring about 20 nm in width. Following sequential annealing at temperatures of 673 K, 723 K, and 773 K, each for 30 minutes, the dimensions of the amorphous layers along the pore edges were notably reduced from about 3 nm to less than 1 nm. Subsequent annealing up to 873 K induced only slight changes, while the sizes and shapes of the nanopores remained unchanged. The presence of a minimal sub-1-nm amorphous edge might represent a limit within the annealing process, possibly due to a minimal amount of inevitable oxidation and hydrogen termination prior to TEM studies. The substantial reduction in pore-edge defects holds significance for achieving desired phonon wave effects within a periodic nanoporous structure.

Supplementary Material: Supplementary material (details of the sample fabrication processes, all the high-resolution TEM images for the pore-edge characterization, pore diameter measurement method, and lattice spacing at each temperature) are available in the online version of this article at http://

Acknowledgements

This work was supported by JST FOREST Program (Grant Number JPMJFR212M), JSPS KAKENHI (Grant No. JP23H01358), and JST CREST Grant Number JPMJCR18I1, Japan. Hao also thanks the support from the Faculty Seed Grant at the University of Arizona.

AUTHOR DECLARATIONS

Conflict of Interest

The authors have no conflicts to disclose.

Author Contributions

Qin-Yi Li: Conceptualization; Methodology; Investigation; Formal analysis; Project administration; Validation; Supervision; Writing – original draft; Funding acquisition. **Fabian Javier Medina:** Methodology; Investigation; Data curation. **Kosuke Kokura:** Methodology; Investigation; Data curation; Formal analysis. **Zheyu Jin:** Methodology; Investigation; Data curation. **Koji Takahashi:** Funding acquisition; Writing – review & editing. **Qing Hao:** Conceptualization; Methodology; Project administration; Validation; Supervision; Writing – original draft; Writing – review & editing; Funding acquisition.

DATA AVAILABILITY

The data that support the findings of this study are available from the corresponding authors upon reasonable request.

References

(1) Maire, J.; Anufriev, R.; Yanagisawa, R.; Ramiere, A.; Volz, S.; Nomura, M. Heat conduction tuning by wave nature of phonons. *Science advances* **2017**, *3* (8), e1700027.

(2) Maldovan, M. Narrow Low-Frequency Spectrum and Heat Management by Thermocrystals. *Physical Review Letters* **2013**, *110* (2), 025902.

(3) Xiao, Y.; Chen, Q.; Ma, D.; Yang, N.; Hao, Q. Phonon Transport within Periodic Porous Structures - From Classical Phonon Size Effects to Wave Effects. *ES Materials & Manufacturing* **2019**, *5*, 2-18. DOI: 10.30919/esmm5f237.

(4) Li, Q.; Hao, Q.; Zhu, T.; Zebarjadi, M.; Takahashi, K. Nanostructured and heterostructured 2D materials for thermoelectrics. *Engineered Science* **2021**, *13*, 24-50. DOI: 10.30919/es8d1136 Scopus.

(5) Li, Q. Y.; Feng, T.; Okita, W.; Komori, Y.; Suzuki, H.; Kato, T.; Kaneko, T.; Ikuta, T.; Ruan, X.; Takahashi, K. Enhanced Thermoelectric Performance of As-Grown Suspended Graphene Nanoribbons. *ACS Nano* **2019**, *13* (8), 9182-9189. DOI: 10.1021/acsnano.9b03521.

(6) Kim, H.; Yun, J.; Gao, M.; Kim, H.; Cho, M.; Park, I. Nanoporous Silicon Thin Film-Based Hydrogen Sensor Using Metal-Assisted Chemical Etching with Annealed Palladium Nanoparticles. *ACS Applied Materials & Interfaces* **2020**, *12* (39), 43614-43623. DOI: 10.1021/acsami.0c10785.

(7) Shi, G.; Kioupakis, E. Electronic and Optical Properties of Nanoporous Silicon for Solar-Cell Applications. *ACS Photonics* **2015**, *2* (2), 208-215. DOI: 10.1021/ph5002999.

(8) Surwade, S. P.; Smirnov, S. N.; Vlassiouk, I. V.; Unocic, R. R.; Veith, G. M.; Dai, S.; Mahurin, S. M. Water desalination using nanoporous single-layer graphene. *Nature Nanotechnology* **2015**, *10* (5), 459-464. DOI: 10.1038/nnano.2015.37.

(9) Garg, J.; Chen, G. Minimum thermal conductivity in superlattices: A first-principles formalism. *Physical Review B* **2013**, *87* (14), 140302.

(10) Ravichandran, J.; Yadav, A. K.; Cheaito, R.; Rossen, P. B.; Soukiassian, A.; Suresha, S. J.; Duda, J. C.; Foley, B. M.; Lee, C.-H.; Zhu, Y.; et al. Crossover from incoherent to coherent phonon scattering in epitaxial oxide superlattices. *Nat Mater* **2014**, *13* (2), 168-172, Letter. DOI: 10.1038/nmat3826 http://www.nature.com/nmat/journal/v13/n2/abs/nmat3826.html#supplementary-information.

(11) Tang, J.; Wang, H.-T.; Lee, D. H.; Fardy, M.; Huo, Z.; Russell, T. P.; Yang, P. Holey Silicon as an Efficient Thermoelectric Material. *Nano Letters* **2010**, *10* (10), 4279-4283. DOI: 10.1021/nl102931z.

(12) Jain, A.; Yu, Y.-J.; McGaughey, A. J. Phonon transport in periodic silicon nanoporous films with feature sizes greater than 100 nm. *Physical Review B* **2013**, *87* (19), 195301.

(13) Ravichandran, N. K.; Minnich, A. J. Coherent and incoherent thermal transport in nanomeshes. *Physical Review B* **2014**, *89* (20), 205432.

(14) Hao, Q.; Xu, D.; Zhao, H.; Xiao, Y.; Medina, F. J. Thermal Studies of Nanoporous Si Films with Pitches on the Order of 100 nm—Comparison between Different Pore-Drilling Techniques. *Scientific Reports* **2018**, *8* (1), 9056.

(15) Lee, J.; Lee, W.; Wehmeyer, G.; Dhuey, S.; Olynick, D. L.; Cabrini, S.; Dames, C.; Urban, J. J.; Yang, P. Investigation of phonon coherence and backscattering using silicon nanomeshes. *Nature communications* **2017**, *8*, 14054.

(16) Klitsner, T.; Pohl, R. Phonon scattering at silicon crystal surfaces. *Physical Review B* **1987**, *36* (12), 6551.

(17) Xu, D.; Wang, Q.; Wu, X.; Zhu, J.; Zhao, H.; Xiao, B.; Wang, X.; Wang, X.; Hao, Q. Largely Reduced Cross-Plane Thermal Conductivity of Nanoporous $In_{0.1}Ga_{0.9}N$ Thin Films Directly Grown by Metalorganic Chemical Vapor Deposition. *Frontiers in Energy* **2018**, 1-10.

(18) Girit, Ç.; Meyer, J. C.; Erni, R.; Rossell, M. D.; Kisielowski, C.; Yang, L.; Park, C. H.; Crommie, M. F.; Cohen, M. L.; Louie, S. G.; et al. Graphene at the Edge: Stability and Dynamics. *Science* **2009**, *323* (5922), 1705-1708. DOI: 10.1126/science.1166999.

(19) Jia, X. T.; Hofmann, M.; Meunier, V.; Sumpter, B. G.; Campos-Delgado, J.; Romo-Herrera, J. M.; Son, H. B.; Hsieh, Y. P.; Reina, A.; Kong, J.; et al. Controlled Formation of Sharp Zigzag and Armchair Edges in Graphitic Nanoribbons. *Science* **2009**, *323* (5922), 1701-1705. DOI: 10.1126/science.1166862.

(20) Li, Q.-Y.; Takahashi, K.; Ago, H.; Zhang, X.; Ikuta, T.; Nishiyama, T.; Kawahara, K. Temperature dependent thermal conductivity of a suspended submicron graphene ribbon. *Journal of Applied Physics* **2015**, *117* (6), Article. DOI: 10.1063/1.4907699.

(21) Wang, H. D.; Hu, S. Q.; Takahashi, K.; Zhang, X.; Takamatsu, H.; Chen, J. Experimental study of thermal rectification in suspended monolayer graphene. *Nature Communications* **2017**, *8*. DOI: 10.1038/ncomms15843.

(22) Hu, S. Q.; Zhang, Z. W.; Jiang, P. F.; Chen, J.; Volz, S.; Nomura, M.; Li, B. W. Randomness-Induced Phonon Localization in Graphene Heat Conduction. *Journal of Physical Chemistry Letters* **2018**, *9* (14), 3959-3968. DOI: 10.1021/acs.jpclett.8b01653.

(23) Hu, S. Q.; Chen, J.; Yang, N.; Li, B. W. Thermal transport transport in graphene with defect and doping: Phonon modes analysis. *Carbon* **2017**, *116*, 139-144. DOI: 10.1016/j.carbon.2017.01.089.

(24) Hao, Q.; Xiao, Y.; Medina, F. J. Annealing Studies of Nanoporous Si Thin Films Fabricated by Dry Etch. *ES Materials & Manufacturing* **2019**, *6*, 24-27. DOI: 10.30919/esmm5f608.

(25) Ma, J.; Wang, S.; Wan, X.; Ma, D.; Xiao, Y.; Hao, Q.; Yang, N. The unrevealed 3D morphological evolution of annealed nanoporous thin films. *Nanoscale* **2022**, *14* (45), 17072-17079, 10.1039/D2NR04014J. DOI: 10.1039/D2NR04014J.

(26) Storm, A. J.; Chen, J. H.; Ling, X. S.; Zandbergen, H. W.; Dekker, C. Fabrication of solid-state nanopores with single-nanometre precision. *Nat Mater* **2003**, *2* (8), 537-540. DOI: 10.1038/nmat941 From NLM.

(27) Jacobsohn*, L.; Cooke, D.; Bennett, B.; Muenchausen, R.; Nastasi, M. Effects of thermal annealing and ageing on porous silicon photoluminescence. *Philosophical Magazine* **2005**, *85* (23), 2611-2620.

(28) Ookubo, N.; Ono, H.; Ochiai, Y.; Mochizuki, Y.; Matsui, S. Effects of thermal annealing on porous silicon photoluminescence dynamics. *Applied physics letters* **1992**, *61* (8), 940-942.

(29) Gayler, M. L. V. Melting point of high-purity silicon. *Nature* **1938**, *142*, 478-478, Letter. DOI: 10.1038/142478a0.

(30) Pan, Y.; Tao, Y.; Qin, G.; Fedoryshyn, Y.; Raja, Y. N.; Hu, M.; Degen, C. L.; Poulikakos, D. Surface Chemical Tuning of Phonon and Electron Transport in Free-Standing Silicon Nanowire Arrays. *Nano Letters* **2016**, *16* (10), 6364-6370, Article. DOI: 10.1021/acs.nanolett.6b02754.

(31) Chang, F. M.; Wu, Z. Z.; Huang, J. H.; Chen, W. T.; Brahma, S.; Lo, K. Y. Migration Energy Barriers for the Surface and Bulk of Self-Assembly ZnO Nanorods. *Nanomaterials* **2018**, *8* (10). DOI: 10.3390/nano8100811.